Correlated growth in ultrathin pentacene films on silicon oxide: Effect of deposition rate

Sirapat Pratontep and Martin Brinkmann*
Institut Charles Sadron CNRS UPR-022, 6 Rue Boussingault, 67083 Strasbourg, France

Frank Nüesch and Libero Zuppiroli
LOMM-IMX-EPFL, Swiss Federal Institute of Technology, CH-1015 Lausanne, Switzerland
(Received 13 November 2003; published 2 April 2004)

Understanding the growth mechanism in molecular organic thin films is fundamental to their applications in organic electronics. We present an extensive study of the growth mechanism of pentacene thin films on silicon dioxide (SiO_2) using atomic force microscopy. For a fixed substrate temperature T_s, the deposition rate κ is found to be a key parameter in controlling the nucleation density in the submonolayer regime and hence transport properties in the first layer of the organic field effect transistors. At a fixed $T_s = 338$ K the maximum number of pentacene islands per unit area N follows the scaling law $N \propto \kappa^{\delta}$ with $\delta = 1.16 \pm 0.10$. A mechanism of homogeneous nucleation followed by diffusive growth accounts for this behavior and allows us to estimate the critical nucleus size of the pentacene islands. The results obtained from a statistical analysis of the island size distribution are fully consistent with a phenomenological capture zone model. The validity of this model depends on the extent of reevaporation of pentacene admolecules during deposition, which is moderated by the deposition rate. We demonstrate that the rate dependence of island nucleation has important implications for the density of grain boundaries, which may play an important role in the transport mechanism.

DOI: 10.1103/PhysRevB.69.165201 PACS number(s): 61.43.Hv, 81.15.Ef, 68.37.Ps, 85.65.+h

I. INTRODUCTION

In an effort to integrate organic semiconductors into electronic devices, ultrathin films consisting of a few molecular layers are raising increasing interest.[1–3] In organic field effect transistors (OFETs) based on organic semiconductors like oligothiophenes and acenes, transport properties have been shown to depend closely on the morphology and the crystal structure of the first few molecular layers in contact with the dielectric layer (SiO_2, Al_2O_3).[3] Accordingly, optimizing OFET performances requires control and understanding of the nucleation and growth mechanism in the submonolayer regime. Organic thin films grown by high vacuum deposition onto clean insulator substrates (Al_2O_3 and SiO_2) presents an ideal case system for this study. Both thermodynamics and kinetics of island formation are controlled by different deposition parameters such as substrate temperature T_s, surface coverage θ, and deposition rate κ as well as the chemical nature and the crystalline structure of the substrate. The overall theoretical framework for homogeneous nucleation and growth based on the rate-equation formalism has been thoroughly developed, especially by Venables *et al.*, and verified experimentally in a number of cases for inorganic systems.[4] Yet there exists only a limited number of studies which applied this theoretical frame to organic systems.[5,6]

In this study, we focus on the early stage of the growth of a molecular semiconductor, i.e., pentacene, on silicon oxide. Pentacene ($C_{22}H_{14}$) is a fully conjugated aromatic molecule consisting of five fused benzene rings. This molecule has recently emerged as a key material in the design of OFETs, with a high charge mobility of the order of 1 $cm^2/V\,s$ and high on/off ratios observed.[7] The coverage range $\theta \leqslant 40\%$ in this investigation corresponds to the nucleation and growth regime where islands are undergoing neither coalescence nor Ostwald ripening.

Our paper is organized as follows. Section II describes experimental conditions for thin film deposition as well as atomic force microscope (AFM) imaging and data processing. Section III is divided into two main subsections. The first part deals with the rate dependence of the total stable island density per unit area, enabling us to estimate the critical nucleus size. The second part focuses on the analysis of domain size distributions. We also demonstrate that the phenomenological capture zone model used in previous studies to model the growth of amorphous Alq_3 domains[6] can be successfully applied to the case of crystalline layers of pentacene in the submonolayer regime under certain conditions of deposition rate.

II. EXPERIMENTAL SECTION

The substrates used in this study consist of a boron doped silicon wafer with a 200-nm-thick thermal oxide layer. No further solution cleaning steps were applied to the silicon/silicon dioxide substrates. Atomic force microscopy measurements on these substrates revealed smooth oxide surfaces with a rms roughness below 0.1 nm. In order to eliminate organic contaminants on the oxide surfaces, we applied a rf oxygen plasma treatment for 5 min in an atmosphere of 10^{-1} mbar pure oxygen. The power density of the plasma was 0.1 W/cm^2 and a bias of -50 V was applied to the substrates. We also performed Kelvin probe measurements inside the vacuum chamber to observe surface potential shifts induced by the oxygen plasma. For this purpose, doped silicon surfaces with a very thin oxide layer were used. The surface potential of 4.9 V was nearly unchanged after the oxygen surface plasma, indicating that the treatment

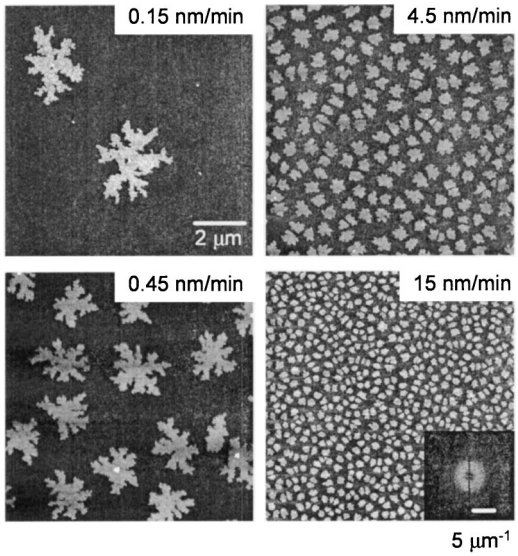

FIG. 1. AFM surface topography of 0.5-nm-thick pentacene films grown at various deposition rates on a 200-nm-thick SiO_2 substrate at a fixed $T_s = 65\,^{\circ}\mathrm{C}$. All the images are $10 \times 10\ \mu\mathrm{m}^2$. Inset: a Fourier transform of the AFM image for the rate 15 nm/min.

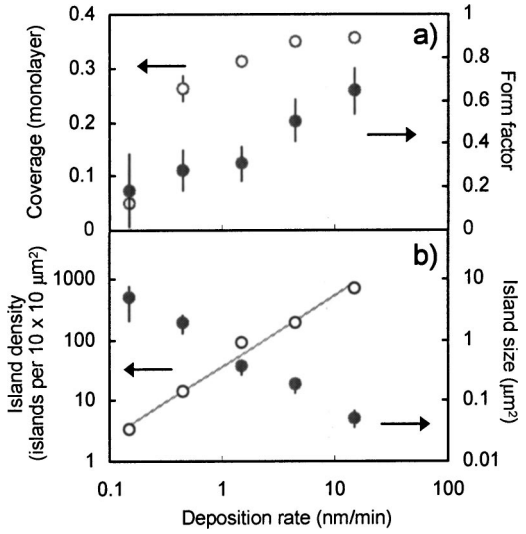

FIG. 2. Dependence of surface morphology on deposition rate κ for pentacene thin films with a nominal thickness of 0.5 nm on SiO_2. (a) The κ dependence of the surface coverage measured by AFM and the form factor f. (b) The κ dependence of the number density of islands N and the mean area of the islands $\langle A \rangle$. The error bars represent the standard deviation for the corresponding size distributions. The dotted line results from a fit using a power law dependence (see text).

does not induce substantial stoichiometric changes of the oxide layer.

High vacuum deposition of pentacene was performed at a base pressure of 3×10^{-7} mbar. Pentacene (Fluka) which had been purified twice by vacuum sublimation was evaporated from a fused quartz crucible heated by a tungsten wire. To investigate the effect of deposition rate on the maximum nucleation density N, we have chosen to work at a fixed substrate temperature $T_s = 338\,\mathrm{K}$ $(65\,^{\circ}\mathrm{C})$. The nominal thickness is measured by a quartz crystal balance kept at 293 K. No reevaporation is observed on the microbalance at 293 K, which ensures the same total amount of material deposited onto SiO_2 for all deposition rates. Topography of the films was investigated by *ex situ* atomic force microscopy on a Nanoscope III in tapping mode using Si tips (25–50 N/m and 280–365 kHz). Statistics of the island size distributions (ISDs) for each deposition rate were obtained on 300–500 islands. ANALYSIS (soft imaging system) software was employed for the statistical analyses of the topographic AFM images. The center coordinates (x_i, y_i) of individual islands were extracted from topographic AFM images for use as input data for Voronoi tesselation performed by VOROGLIDE software[8] in the analysis of the capture zone model.

III. RESULTS

A. Nucleation and role of reevaporation

Figure 1 depicts typical topographic AFM images of 0.5-nm-thick pentacene layers grown at various deposition rates on a SiO_2 substrate at $T_s = 338\,\mathrm{K}$. In all cases, pentacene is observed to form islands with a typical height of approximately 1.5 ± 0.1 nm corresponding to a monolayer of pentacene molecules slightly inclined to the normal of the substrate.[9] The spatial distribution of the islands is clearly different from a random Poisson seeding. The existence of strong spatial correlations is evidenced by the fast Fourier transform (FFT) of the topographic images (see inset of Fig. 1). The FFT in Fig. 1 clearly shows a ring whose radius corresponds to the correlation distance between nearest neighbor islands, λ_{NN}. Note also the uniformity in domain sizes, especially for deposition rates κ above 1 nm/min. This narrow size distribution indicates that secondary nucleation between islands has not occurred during growth, underlining the existence of extended depletion zones around existing nuclei that hinder secondary nucleation. For $\theta \leqslant 40\%$, coalescence events between neighboring domains are insignificant. We emphasize that the cleanliness of the substrates achieved after the plasma treatment is of utmost importance in order to avoid heterogeneous nucleation of three-dimensional (3D) crystals initiated by surface impurities.

Figure 1 reveals three interesting trends as a function of increasing κ for constant nominal thickness and substrate temperature: (i) the apparent coverage θ of the SiO_2 substrate increases, (ii) the morphology of the islands becomes more compact, and (iii) the number density of islands is found to increase and accordingly the domain size to decrease.

In Fig. 2(a), the observed coverage θ for samples with the same nominal thickness 0.5 nm is plotted as a function of increasing rate κ. This shows that θ first increases with κ and saturates to a limiting value of approximately 0.35 monolayers. The asymptotic limit $\theta_{\max} = 0.35$ at high deposition rate is fully consistent with the expected value for complete condensation $\theta = h/h_{mono} = 0.33$ (using the monolayer thickness $h_{mono} \approx 1.5$ nm). The increase of coverage for increasing deposition rate is a clear indication of reevaporation during deposition, particularly at low deposition rates. Qualitatively,

we explain that, for low deposition rates, admolecules have to diffuse for a larger distance on the substrate before being incorporated into islands because of the low nucleus density, hence having a larger probability of being desorbed (see Sec. IV).

The compactness of an island can be quantified by using a form factor f. In Fig. 2(a), we also plot the form factor $f=4\pi\langle A\rangle/\langle P\rangle^2$ where $\langle A\rangle$ and $\langle P\rangle$ are the mean area and the mean perimeter of the islands.[10] Clearly, the branched dendritic structures observed at low κ lead to low values of f (below 0.2) which tends toward 0.65 at high rates of more than 10 nm/min. As pointed out by Tromp and co-workers, the branched dendritic morphology is indicative of diffusion limited aggregation.[2] The limit $f\rightarrow 0$ is expected for a fractal object with fractal dimension $d=1.6-1.7$. Even at the high rates, the form factor remains below the limit $f=1$ for circular islands.

Figure 2(b) illustrates the κ dependence of the density of islands per unit surface N, together with that of the average island size. The plotted data correspond approximately to the maximum island density observed in the apparent coverage range 0.2–0.4, where coarsening (coalescence and ripening) is negligible (for the rate 0.15 nm/min, the maximum N is observed for the film of approximately 1.0 nm nominal thickness). In the case of SiO_2 substrate, we observe that $N\propto\kappa^{\delta}$ with $\delta=1.16\pm0.10$ for κ varying over two orders of magnitude (0.15 nm/min to 45 nm/min). As demonstrated by Venables and co-workers,[4] in the case of homogeneous nucleation the density of stable islands N is expected to vary (i) as a power law with the deposition rate κ and (ii) as an activated Arrhenius law with the substrate temperature T_s:

$$N\propto\kappa^{\delta}\exp(\beta E_N) \tag{1}$$

where E_N is the activation energy for homogeneous nucleation and $\beta=(k_BT_s)^{-1}$. E_N is a function of the activation energy for desorption E_A and the free energy difference E_i between i molecules in the island and in the adsorbed state, and E_D is the activation energy for surface diffusion of pentacene molecules. Note that i denotes the critical nucleus size where an island of i molecules is the most unstable and will dissociate. Stable islands start to grow from size $i+1$.

Different regimes of condensation (complete, initially incomplete and totally incomplete) lead to different power laws of N as a function of κ.[4] In the case of complete condensation for 2D islands, one expects $\delta=i/(i+2)<1$.[4] For complete condensation, our experimental value of the exponent $\delta\approx1$ would be the asymptotic limit for an extremely large critical nucleus size i. We discard this possibility, given the evidence for reevaporation, which implies a regime of incomplete condensation, at least up to $\kappa=15$ nm/min. Two regimes of incomplete condensation have been distinguished by Venables and co-workers in the case of 2D islands, namely, (i) extreme incomplete condensation which yields $\delta=i$ and $E_N=[E_i+(i+1)E_A-E_D]$ and (ii) initially incomplete condensation which gives $\delta=i/2$ and $E_N=(E_i+iE_A)/2$. In the former regime, clusters grow upon direct incorporation of impinging molecules on the cluster surface, whereas in the latter cluster growth is mainly controlled by diffusion of molecules on the substrate surface. In the present case, we consider that the initially incomplete condensation applies. Indeed, in the case of extreme incomplete condensation, one would expect the apparent coverage to be a fraction of the deposited thickness in all cases.[11] Moreover, the fractal morphology of domains at low deposition rates indicates that the growth proceeds by diffusion of admolecules in a diffusion limited aggregation (DLA) regime. Accordingly, we estimate the critical nucleus size to be two pentacene molecules, i.e., clusters with size $i\geqslant3$ will be stable whereas clusters of two molecules will have a larger probability of dissociation.

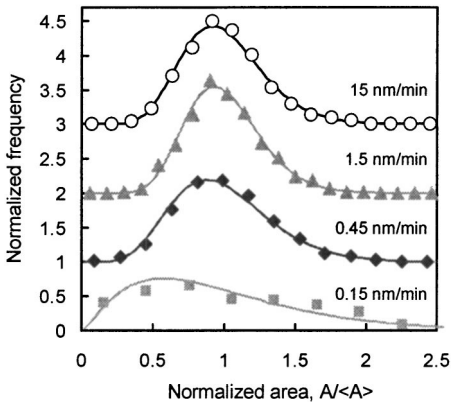

FIG. 3. Comparison of the island size distributions for four different deposition rates. The results are fitted to a Gamma distribution. The ordinate axis represents the scaled variable $x=A/\langle A\rangle$.

We emphasize that the determination of the critical nucleus size i relies strongly on the growth model chosen to describe the nucleation and growth mechanism and the employed methodology. For instance, in Ref. 12 a value $i=3$ was obtained for pentacene islands at 293 K from the fitting of the ISD using the analytical form predicted by the model of Amar and Family.[13] In this model, condensation is assumed to be complete and the fitting parameter of the ISD depends directly on the critical nucleus size i. A different approach for the determination of i which we have adopted here involves (i) the identification of the condensation regime at work and (ii) the determination of the scaling law in Eq. (1).[4,11] However, as stated by Venables *et al.*, in the so-called ''initially incomplete'' regime of condensation, the exact power-law dependence of the nucleation density N on the deposition rate κ may need to be resolved by numerical simulations.[4]

B. Analytical form of the island size distributions

A closer insight into the growth of pentacene in the submonolayer regime has been obtained by analyzing the size distributions as a function of deposition rate. In Fig. 3, we depict typical island size distributions for κ in the range 0.15–15 nm/min. We can distinguish two regimes for the ISD. For $\kappa\leqslant0.15$ nm/min, the ISD is found to be extremely broad, whereas, for $\kappa\geqslant0.45$ nm/min, the ISD is narrow and has a positive skewness. This skewness is not due to coalescence of neighboring islands, given the low substrate cover-

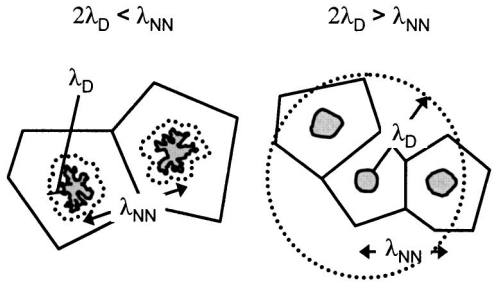

FIG. 4. Schematic showing the effect of the interplay between the mean intergrain distance λ_{NN} and the diffusion distance λ_D on the growth mechanism in the submonolayer regime of pentacene. In the case $2\lambda_D<\lambda_{NN}$, the capture zones of the islands are delimited by the dotted lines, whereas for $2\lambda_D>\lambda_{NN}$ they coincide with the polygonal Wigner-Seitz cells (see text).

age (see above), but represents an intrinsic characteristic of the ISD. The overall form of the ISD observed for pentacene islands is similar to that evidenced in the case of Alq_3/H-passivated Si(100).[6] In this case, the ISD was shown to be consistently described by a Gamma distribution:

$$G_p(x)=\frac{p^p}{\Gamma(p)}x^{p-1}\exp(-px), \tag{2}$$

where $x=A/\langle A\rangle$ is the normalized variable and p is defined as

$$p=\frac{\langle A\rangle^2}{\sigma^2} \tag{3}$$

for a χ^2 distribution. $\langle A\rangle$ is the mean value and σ^2 is the variance of the island size distribution.

This analytical form of the ISD follows from a capture zone (CZ) model proposed by Mulheran and Blackman.[14] With respect to the classical growth models based on the rate-equation formalism, this model takes into account the correlated nature of growth between neighboring islands by including the local environment of each island.[14] The principal assumption of the CZ model is that existing nuclei grow at a rate which is proportional to their capture zone areas A_{CZ}, which are delimited by polygonal cells built on the seeds of nuclei (see Fig. 4). These cells can be determined by Voronoi tessellation and the analytical distribution of cell areas is of the Gamma type. The scaling of the ISD versus coverage stems from the invariance of the Voronoi network.[14]

We have fitted the experimental ISD to a Gamma distribution using a maximum log-likelihood method.[15] Figure 3 illustrates the close matching obtained for $\kappa\geqslant 0.45$ nm/min. However, we emphasize that the identification of the analytical form of the ISD may remain ambiguous from only the fitting of the experimental data and necessitates a thorough analysis of the various moments of the ISD.

To ascertain the Gamma form of the distribution, we compare in Table I the values of p obtained from Eq. (3) (i.e., by calculating the first and second moments of the ISD) with those obtained from the previous fitting. A clear matching is observed between the p values extracted by the two different methods, which proves the Gamma form of the distribution. Thus this fitting procedure is fully self-consistent [it would be sufficient to fit the experimental ISD to a Gamma function by only using the p value obtained by Eq. (3)].

TABLE I. Comparison between the values of p from the experimental fitting to the Gamma distribution and the expected values for a χ^2-type distribution.

Deposition rate (nm/min)	$\langle A\rangle/\sigma^2$ (Island size)	p (Gamma fit)
0.45	8.8	8.0 ± 0.8
1.5	14.2	14.0 ± 1.1
4.5	13.4	13.7 ± 1.0
15	11.8	11.9 ± 0.9

For $\kappa\geqslant 0.45$ nm/min, the overall values of p are rather high (>8) and clearly distinct from the value of 3.6 expected for a random Poisson distribution of the nuclei.[16] This is a consequence of strong spatial correlations in the positions of pentacene nuclei on the substrate as evident in the FFT (see Fig. 1). This result highlights the correlated nature of growth between neighboring pentacene islands, which results in a coupling between island positions and sizes and thus supports growth by the CZ model. In contrast, for $\kappa\leqslant 0.15$ nm/min, the ISD hardly matches a Gamma-type distribution.

C. Validity of CZ model vs deposition rate

To investigate the validity of the capture zone model, we performed Voronoi tessellation[6,14] on topographic AFM images in order to verify the main assumption of the CZ model (see above). Figure 5(a) depicts a typical Voronoi pattern built on the (x_i,y_i) center coordinates of pentacene islands for a film deposited at $\kappa=1.5$ nm/min. The proportionality between the area of individual capture zones A_{CZ} and the corresponding area A of the islands is depicted in Fig. 5(b). The strong correlation between A and A_{CZ} is evident and results in a very small dispersion of the data points (correlation coefficient 0.93). The curve $A=\alpha A_{CZ}$ yields a slope $\alpha=0.31$, in agreement with the coverage $\theta=0.33$, since by definition $\langle A\rangle/\langle A_{CZ}\rangle=\theta$. Accordingly, for $\kappa=1.5$ nm/min, the CZ model does clearly apply.

This Voronoi analysis was applied to all the samples grown at different deposition rates to extract the CZ area distributions. In Fig. 6(a), we compare the ISD and the A_{CZ} distribution for two different deposition rates. Whereas a good matching between the two distributions is observed for $\kappa=15$ nm/min, there is a pronounced discrepancy for the rate of 0.15 nm/min. This is further illustrated in Fig. 6(b), showing the κ dependencies of both the values of p characterizing the ISD and the values of p_{CZ} from the CZ area distributions. We observe that p increases from less than 3.0 at $\kappa=0.15$ nm/min to 14.0 at $\kappa=1.5$ nm/min, whereas p_{CZ} remains in all cases above 13. Accordingly, the difference $p_{CZ}-p$ is minimal for the higher rates. This means that only for the higher rates do the island size and CZ area distribu-

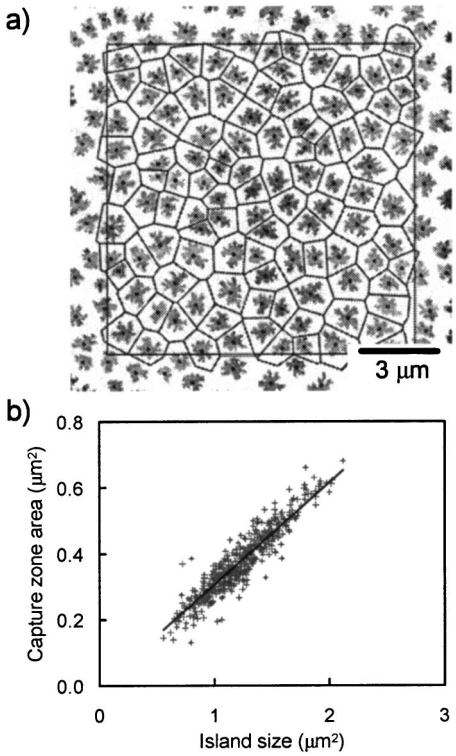

FIG. 5. Capture zone analysis by Voronoi tessellation. (a) Typical Voronoi pattern obtained from the tessellation of a topographic AFM image (deposition rate 1.5 nm/min). (b) Correlation plot between the area A of the islands and the corresponding capture zone area A_{CZ} for each particle. The full line is the result of a linear fit, illustrating the proportionality between CZ area A_{CZ} and island size A.

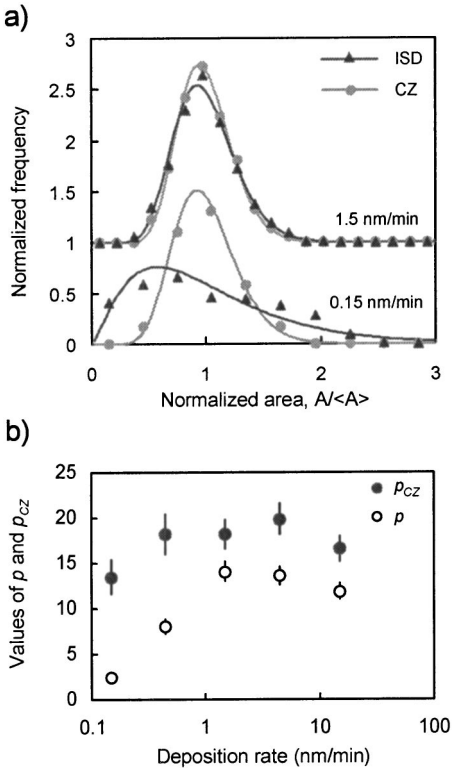

FIG. 6. Validity of the capture zone model as the deposition rate varies. (a) Comparison between the island size distribution and the capture zone area distribution obtained by Voronoi tessellation for $\kappa = 0.15$ nm/min and 4.5 nm/min. The full lines correspond to the best fits using a Gamma distribution. (b) Variation of the values of p for ISD and p_{CZ} for CZ with the deposition rate.

tions coincide. These results underline that the validity of the CZ model is dependent on the deposition rate as discussed in the following section.

IV. DISCUSSION

A. Interplay between surface diffusion and reevaporation of pentacene

The various experimental observations concerning the effect of deposition rate on coverage, form factor, and island size distributions can be interpreted in terms of a balance between λ_{NN}, the mean nearest neighbor (NN) island distance, and λ_D, the mean distance λ_D that a pentacene admolecule diffuses before being desorbed.[11] λ_D is given by $\lambda_D = \sqrt{D\tau_A}$, where D is the diffusion constant of pentacene molecules on the substrate and τ_A is the mean residence time of pentacene molecules on the substrate.[11] While λ_{NN} varies as $N^{-1/2}$ and hence $\kappa^{-1/2}$, λ_D is expected to stay constant at a fixed T_s. Accordingly, we can distinguish two growth behaviors as a function of deposition rate: (i) $2\lambda_D < \lambda_{NN}$ and (ii) $2\lambda_D > \lambda_{NN}$.

For low deposition rates, i.e., when $2\lambda_D < \lambda_{NN}$, admolecules arriving on the surface far from existing nuclei (see Fig. 4) have a larger probability of reevaporation due to longer diffusion paths before reaching an island. Accordingly, the amount of admolecules incorporated into a given island is no longer determined by the geometrical area of its Wigner-Seitz (WS) cell but depends on the island morphology and diffusion length λ_D. As shown in Fig. 4, at a given moment in the growth regime, the CZ will be roughly defined as the area inside the dotted line extending by $\lambda_D = \sqrt{D\tau_A}$ from the border of the dendritic island. This has several implications. First, the main assumption of the CZ

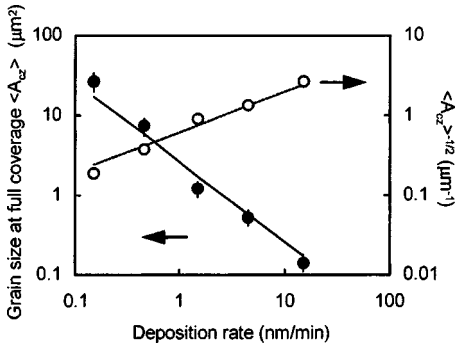

FIG. 7. Evolution of the expected mean island size at full coverage $\langle A_{CZ}\rangle$ and the estimate of the grain boundary density $\langle A_{CZ}\rangle^{-1/2}$ with the deposition rate. The lines are the best fits for power laws with the exponent values of -1 for $\langle A_{CZ}\rangle$ and 0.5 for $\langle A_{CZ}\rangle^{-1/2}$.

model which implies proportionality between the growth rate of an island and its CZ area defined as the WS cell is no longer verified. Second, in the absence of overlap between adjacent CZs, NN islands tend to grow in a noncorrelated manner. This leads to broadened island size distributions and the fractal island morphology typical for DLA. This case corresponds to $\kappa \leqslant 0.15$ nm/min [see Fig. 6(a)].

For $2\lambda_D > \lambda_{NN}$, diffusive areas of NN islands tend to overlap as schematized in Fig. 4. As a consequence, the CZs of islands are determined by the local environments of each island and can be defined as the Wigner-Seitz cells built on the seeding of surrounding nuclei. This ensures the correlated nature of growth between NN domains and thus leads to narrow Gamma-type ISDs and nonrandom spatial distributions. An equilibrium concentration of admolecules between the islands develops during growth and ensures more compact island morphologies (form factors closer to 1).[11]

B. Implications for the transport properties

The results obtained from the rate dependence of N and the validity of the CZ model have important consequences on transport properties across adjacent pentacene islands in the case of full coverage, since interisland boundaries are expected to contain a larger concentration of traps for charge carriers.[17] At full coverage, a good approximation of these grain boundaries is obtained from the Voronoi mosaic built on the initial seeding of nucleation centers. Thus the grain size and the total length of grain boundaries per unit area between pentacene islands is mainly determined by the spatial distribution of nucleation centers.

In Fig. 7, we have plotted both the mean grain size $\langle A_{CZ} \rangle$ and the total amount of grain boundaries per unit area, which is by first approximation proportional to $\langle A_{CZ} \rangle^{-1/2}$.[18] We see that the change of deposition rate from 0.15 nm/min to 15 nm/min results in an increase of more than one order of magnitude in the grain boundary density. Accordingly, one expects a sizable increase of the concentration in charge carrier traps and hence a decrease of the carrier mobility. Therefore, the deposition rate is potentially one of the key factors essential to the improvement of charge carrier mobilities in ultrathin pentacene films, in addition to polymorphism, structural defects within islands, and chemical impurities.

V. CONCLUSIONS

This study demonstrates that systems involving organic semiconductors on atomically flat and inert substrates like SiO_2 are ideal to probe the validity of theoretical growth models. In the case of inorganic systems, this is often complicated by experimental factors such as surface defects. Several important aspects of the nucleation and growth in the early stage of deposition of pentacene onto SiO_2 have been unveiled. The nucleation density N varies almost linearly with deposition rate κ at a fixed substrate temperature $T_s = 338$ K. The rate-equation formalism explains this scaling and allows us to estimate the critical nucleus size. Condensation occurs in the incomplete regime due to reevaporation, especially at low deposition rates $\kappa \leqslant 0.45$ nm/min. The island size distributions are consistently described by a Gamma function characterized by a single parameter p which varies with deposition rate. For $\kappa \geqslant 1.5$ nm/min, large p values indicate correlated growth of nearest neighbor islands, which are evidenced by the existence of a well defined nearest neighbor distance λ_{NN}. The interplay between λ_{NN} and the mean diffusion distance λ_D is shown to control the degree of correlations. Correlated growth is observed for $2\lambda_D > \lambda_{NN}$ and is successfully described by the capture zone mechanism proposed by Blackman and Mulheran. Further investigations will focus on the role of reevaporation at different substrate temperatures and the determination of the activation energies for surface diffusion and reevaporation.

In addition, we have demonstrated that the rate dependence of the nucleation density has strong implications on the density of grain boundaries per unit area, which is one of the limiting factors for the carrier mobility in OFET structures. The characterization of OFETs versus deposition rate will be the subject of a future communication. In particular, it would be interesting to probe the molecular ordering within the dendritic islands and its impact on the charge carrier mobility.

ACKNOWLEDGMENTS

We acknowledge support by EEC Contract No. HPRN-CT-2002-0327 and the Swiss National Science Foundation under Contract No. 20-67929.02.

*Email address: brinkmann@ics.u-strasbg.fr

[1] D. E. Hooks, T. Fritz, and M. D. Ward, Adv. Mater. (Weinheim, Ger.) **13**, 227 (2001); C. D. Dimitrakopoulos and P. L. Malenfant, *ibid.* **14**, 99 (2002).

[2] J. F. Meyer zu Heringdorf, M. C. Reuter, and R. M. Tromp, Nature (London) **412**, 517 (2001).

[3] A. Dodabalapur, L. Torsi, and H. E. Katz, Science **268**, 270 (1995); E. L. Granström and C. D. Frisbie, J. Phys. Chem. B **103**, 8842 (1999).

[4] J. A. Venables, G. D. T. Spiller, and M. Hanbücken, Rep. Prog. Phys. **47**, 399 (1984).

[5] F. Biscarini, R. Zamboni, P. Samori, P. Ostoja, and C. Taliani, Phys. Rev. B **52**, 14 868 (1995); R. Ruiz, B. Nickel, N. Koch, L. C. Feldman, R. F. Haglund, A. Kahn, and G. Scoles, *ibid.* **67**, 125406 (2003).

[6] M. Brinkmann, F. Biscarini, C. Taliani, I. Aiello, and M. Ghedini, Phys. Rev. B **61**, R16 339 (2000); M. Brinkmann, S. Graff, and F. Biscarini, *ibid.* **66**, 165430 (2002).

[7] D. J. Gundlach, Y. Y. Lin, T. N. Jackson, S. F. Nelson, and D. G. Schlom, IEEE Electron Device Lett. **18**, 87 (1997).

[8] C. Icking, R. Klein, P. Köllner, and L. Ma, computer code VOROGLIDE, Fern Universität Hagen, 1996–1997.

[9] C. Dimitrakopoulos, A. Brown, and A. Pomp, J. Appl. Phys. **80**, 2501 (1996); M. Brinkmann, S. Graff, C. Straupé, J.-C. Wittmann, C. Chaumont, F. Nüesch, A. Aziz, M. Schaer, and L. Zuppiroli, J. Phys. Chem. B **107**, 10 531 (2003).

[10] The form factor f measured by AFM is affected by the convolution of the real island geometry with the tip shape. Accordingly, the measurements may overestimate the values of f.

[11] P. Jensen, Rev. Mod. Phys. **71**, 1695 (1999), and references therein.
[12] R. Ruiz, B. Nickel, N. Koch, L. C. Feldman, R. F. Haglund, A. Kahn, F. Family, and G. Scoles, Phys. Rev. Lett. **91**, 136102 (2003).
[13] J. G. Amar and F. Family, Phys. Rev. Lett. **74**, 2066 (1995).
[14] P. A. Mulheran and J. A. Blackman, Philos. Mag. Lett. **72**, 55 (1995); Phys. Rev. B **53**, 10 261 (1996).
[15] J. Mathews and R. L. Walker, *Mathematical Methods of Physics* (W. A. Benjamin, London, 1970), p. 387.
[16] D. Weaire and N. Rivier, Contemp. Phys. **25**, 59 (1984).
[17] E. A. Silinsh, *Organic Molecular Crystals* (Springer, Berlin, 1980), pp. 139–220; G. Horowitz and A. Hajlaoui, Adv. Mater. (Weinheim, Ger.) **12**, 1046 (2000).
[18] Since the grain boundary length is proportional to $\langle A_{CZ}\rangle^{1/2}$, the grain boundary length per unit area equals $\langle A_{CZ}\rangle^{1/2}/\langle A_{CZ}\rangle$ multiplied by a geometrical factor depending on the shape and the spatial distributions of the grains. Since the Gamma distributions of CZ are similar at all deposition rates, we may assume that this geometrical factor does not change significantly with the rate.